Silicon based nanogap device for studying electrical transport phenomena in molecule–nanoparticle hybrids

2008 J. Phys.: Condens. Matter 20 374126

(http://iopscience.iop.org/0953-8984/20/37/374126)

J. Phys.: Condens. Matter **20** (2008) 374126 (6pp) doi:10.1088/0953-8984/20/37/374126

Silicon based nanogap device for studying electrical transport phenomena in molecule–nanoparticle hybrids

Sebastian Strobel[1], **Rocío Murcia Hernández**[1], **Allan G Hansen**[2] **and Marc Tornow**[2,3]

[1] Walter Schottky Institut, Technische Universität München, Am Coulombwall 3, 85748 Garching, Germany
[2] Institut für Halbleitertechnik, Technische Universität Braunschweig, Hans-Sommer-Straße 66, 38106 Braunschweig, Germany

E-mail: m.tornow@tu-bs.de

Received 15 February 2008, in final form 31 March 2008
Published 26 August 2008
Online at stacks.iop.org/JPhysCM/20/374126

Abstract
We report the fabrication and characterization of vertical nanogap electrode devices using silicon-on-insulator substrates. Using only standard silicon microelectronic process technology, nanogaps down to 26 nm electrode separation were prepared. Transmission electron microscopy cross-sectional analysis revealed the well defined material architecture of the nanogap, comprising two electrodes of dissimilar geometrical shape. This asymmetry is directly reflected in transport measurements on molecule–nanoparticle hybrid systems formed by self-assembling a monolayer of mercaptohexanol on the electrode surface and the subsequent dielectrophoretic trapping of 30 nm diameter Au nanoparticles. The observed Coulomb staircase I–V characteristic measured at $T = 4.2$ K is in excellent agreement with theoretical modelling, whereby junction capacitances of the order of a few 10^{-18} farad and asymmetric resistances of 30 and 300 MΩ, respectively, are also supported well by our independent estimates for the formed double barrier tunnelling system. We propose our nanoelectrode system for integrating novel functional electronic devices such as molecular junctions or nanoparticle hybrids into existing silicon microelectronic process technology.

1. Introduction

The ongoing miniaturization of electronic devices in integrated circuits [1] has led to increased activity in the research and development of novel electronic units which eventually may replace current silicon microelectronics. In this regard, organic molecules are currently one of the candidates being investigated most intensively [2]. The immediate and complete replacement of full integrated circuits by, e.g. molecules, however, seems unlikely due to the largely unsolved problem of chemical synthesis and the assembly of complex organic networks. These challenges already appear when just simple binary logic functions are to be replaced by molecules [3]. The step-by-step replacement of certain electronic functions only seems more probable at present. In such a 'hybrid' approach most electronic functions would at first remain in standard silicon microelectronic planar technology. Then, on the same chip, nanoscale contact elements would be realized, facilitating the electrical contacting of molecules that take over dedicated electronic functions. In the past, several different methods have been reported to successfully contact single molecules or entire layers and measure their electronic transport properties [4]. However, for most of these the problem of integration into current silicon process technology remains unsolved. Ideally, for integrating a nanoscale contact device which allows for the electrical connection to molecules, we should use the same silicon microelectronic process technology on the same silicon substrate, i.e. it should be integrated in a monolithic manner. One approach addressing these demands is the fabrication of *vertical nanogap electrode devices* (VNDs) based on semiconductor/insulator layered structures, as has been reported before using III–V semiconductors [5–7], bare silicon [8] and metal-coated silicon electrodes [9, 10].

[3] Author to whom any correspondence should be addressed.

In this paper we report on the fabrication technology for VNDs with electrode separation of the order of 20 nm. The preparation is based on silicon-on-insulator (SOI) substrates having a 20 nm thick buried SiO_2 layer and is fully compatible with silicon microelectronic process technology. As test system for the characterization of the electrical properties of nanoscale objects, we dielectrophoretically trapped gold nanoparticles across the electrodes that had been functionalized with a self-assembled monolayer (SAM) before. Low temperature I–V characteristics reveal a pronounced staircase-like behaviour, indicating single electron transport phenomena through the created double barrier tunnelling system. Theoretical model fits in the framework of classical Coulomb blockade theory agree very well with our data. The well defined metal electrode architecture, as characterized in cross-sectional transmission electron microscopy, allows for a quantitative and independent estimate of most of the model fit parameters. In particular, the observed asymmetry in tunnelling junction resistances can be understood this way.

2. Experiment

2.1. Device preparation

Vertical nanogap devices were fabricated from silicon-on-insulator (SOI) wafers (6 inch diameter, 400 μm handle wafer, 20 nm buried SiO_2, 5 μm silicon device layer, resistivity 1–10 Ω cm, purchased from Si-Mat, Landsberg/Lech, Germany). Before processing the wafer it was cut in 9×9 mm^2 pieces by wafer sawing. Each sample piece was subsequently cleaned in acetone, isopropanol and piranha solution (freshly prepared 1:2 mixture of hydrogen peroxide and sulfuric acid, 15 min) to remove all organic residues on the surface. *Note: piranha solution must be handled with care: it is extremely oxidizing, reacts violently with organics and should only be stored in loosely tightened containers to avoid pressure build up*. The nanogap device preparation process following these cleaning steps is schematically outlined in figure 1.

Plateau-like mesa structures were prepared as displayed in figure 1(b) using conventional photolithography and reactive ion etching (RIE). To obtain a sufficiently stable etch mask for the first RIE step, the sample was spin-coated twice using photoresist (Shipley S1818, 6000 rpm, 30 s) leading to an overall resist thickness of $\sim$3 μm. The etching was performed within an Oxford 'Plasmalab 80 Plus' RIE reactor with inductively coupled plasma (ICP) and reactive gases C_4F_8 and SF_6 (mixture 3:2, etching pressure 15 mTorr, temperature 10 °C, power 15 W (RF) and 220 W (ICP)). During the first RIE step typically 20 plateaus of lateral dimension 150 μm were formed, each 3 μm in height. Here, we carefully adjusted the etching depth such that the thin oxide layer was just completely exposed as shown in figure 1(b). Due to a difference in etch rates for silicon and silicon dioxide of approximately 10:1 for the used process a lateral displacement within the etching profile of the upper and lower silicon layer occurs just at the position of the buried oxide, resulting in a terrace of about 100 nm lateral depth. As the next step, the accessible silicon oxide was recess etched in the horizontal direction by dipping the sample for 8 min in 5% hydrofluoric

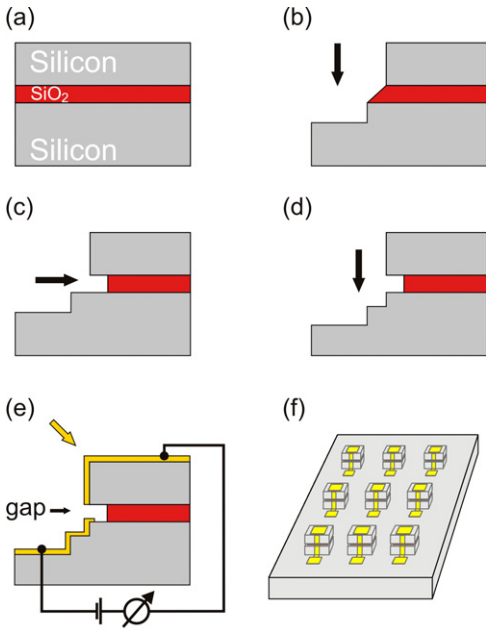

Figure 1. Schematic diagram of VND fabrication. (a) Silicon on insulator substrate with 20 nm buried oxide as base material. (b) Patterning of the sample surface by reactive ion etching (RIE). Due to the difference in etch rates for silicon and silicon dioxide a lateral displacement within the etching profile arises. (c) Selective recess etching of the exposed, thin oxide layer by hydrofluoric (HF) acid. (d) Additional RIE step to improve the co-planarity of the exposed side wall. (e) Angular thin film metal deposition. (f) Array of plateau-like, individually addressable devices.

(This figure is in colour only in the electronic version)

(HF) acid solution, cf figure 1(c). Due to the extremely high selectivity of HF in etching silicon oxide with respect to silicon, a trench featuring exactly the width of the oxide layer is formed. The estimated trench depth was of the order of 300–500 nm. After wet etching, the sample was rinsed in deionized water for 3 min twice and subsequently dried in a N_2 flow. To remove the displacement between the upper and lower silicon layer we carried out a second RIE step, as sketched in figure 1(d). The resulting, steeper side wall shape improves the co-planarity of the later formed metal electrodes and facilitates routine inspection of the gap topology in scanning electron microscopy (SEM), particularly under small viewing angles below 10°. Due to the isotropic component of this etching process the trench width close to the opening is slightly enlarged. Afterwards, 120 μm size contact pads (Ti/Au 10/210 nm) were deposited by e-beam evaporation on top of the plateau structures, as well as down in the etched plane close to the plateaux, as pads for later wire bonding (not shown in figure 1). Finally, the actual nanogap electrodes were formed by depositing a metal layer a few nanometres thick by e-beam evaporation, whereby the evaporation direction was rotated by 45° with respect to the surface normal. Due to a shadow effect at the upper silicon edge the metal layer rips off at the trench as shown in figure 1(e). This deposition proved to be one of the most subtle steps since an optimal balance between sufficiently high lead conductance and small gap separation had to be found. Typically, a metal layer thickness of 10 Å titanium and

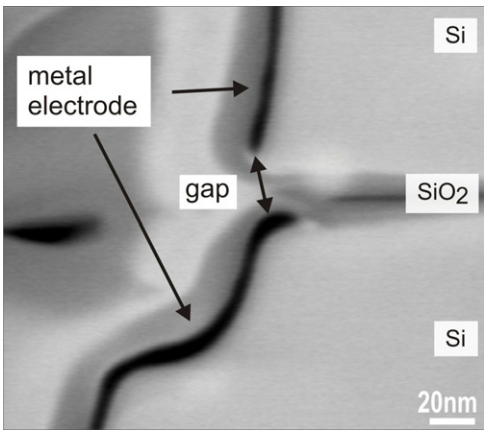

Figure 2. STEM cross-sectional image of the central region of a complete nanogap device as prepared by FIB milling. The evaporated thin film metal layer formed two electrodes of different geometrical shape, visible as dark layers. The FIB/STEM analysis was performed at the application labs of Zeiss SMT AG, Oberkochen, Germany.

85 Å gold was used leading to an overall metal layer thickness of about 10 nm. The 45° angular evaporation ensured that both the plateau top surface and the nanogap electrode planes on the plateau wall were covered with metal at the same time. We used either the complete plateau side wall as electrode or restricted the lateral width by an additional photoresist mask applied prior to evaporation (not included in figure 1). Widths between 5 and 20 μm were tested using negative photoresist (AZ nLOF 2070, Microchemicals). The resist was removed after evaporation by a standard lift-off process in acetone.

2.2. Device characterization

For a thorough and detailed characterization of the material layer composition and thicknesses that comprise the nanogap electrodes we investigated the cross-sectional profile in transmission electron microscopy (TEM). For this purpose, a 100 nm thin lamella was prepared using focused ion beam (FIB) techniques and transferred to a scanning TEM (STEM) sample holder using the so-called lift-out procedure. Figure 2 shows a STEM image of a VND prepared completely in parallel (same sample chip) to the one investigated in transport measurements as described below.

The nanogap as formed between the upper and lower metal layer (visible as dark lines) can be clearly identified. Its measured separation is approximately 26 nm. Due to metal evaporation from an angular direction both electrodes feature different geometrical cross-sections: the upper sharp electrode opposes the lower rounded one. Note also how the horizontal silicon layer displacement has shifted from the gap plane down to approximately 100 nm below the gap as a result of the second RIE step. This way, both electrodes directly oppose each other.

2.3. Electrical setup

For electrical transport measurements the samples were mounted into ceramic chip carriers using gallium as adhesive and Au wire bonding. Gallium provides both a mechanically stable and good thermal contact to the carrier. For low-temperature measurements, the sample was inserted into a custom-made, shielded measurement rod which was evacuated to a pressure below 1 mbar. The rod was subsequently inserted into a He4 dewar vessel and thermally equilibrated by letting in a small amount of He gas (10 mbar). Current–voltage (I–V) characteristics were taken using a Keithley 2400 source meter, controlled via a PC (LabView software). Prior to any electrode functionalization with molecular layers and gold nanoparticles, all electrode pairs of a given sample were electrically characterized at $T = 4.2$ K. Only those samples were considered for further investigation which showed clear isolating behaviour with resistances of at least 20 GΩ, at bias voltages up to a few volts. During all handling, special care was taken to avoid electrostatic discharge induced damage of the sample by connecting all unused chip carrier pins to a common potential.

3. Results

3.1. Electrode functionalization with self-assembled monolayers and gold nanoparticles

For molecular electrode functionalization the sample was cleaned with deionized water (DI) and immersed in 1 mM aqueous mercaptohexanol (MCH) solution to build up a self-assembled monolayer (SAM) [11] on the gold electrode surface. The short alkyl backbone molecule MCH is known to spontaneously form stable and dense monolayers with a film thickness of ∼1.0 nm [12]. After one hour of assembly the sample was flushed with DI water and subsequently dried in a stream of nitrogen. Reference measurements at low temperatures confirmed that the molecular functionalization alone did not affect the device's electrical properties.

Subsequent to SAM functionalization, we bridged the gap between both coated electrodes by dielectrophoretically trapping gold colloid nanoparticles of diameter 30 nm from an aqueous solution of concentration 10^{11} ml^{-1} (Polysciences Europe GmbH, Eppelheim, Germany). The technique of ac dielectrophoretic trapping has been described before, see, e.g. [13] and [14] for a recent detailed description. The parameters employed to obtain optimal trapping results strongly depend on the particular electrode geometry and electrical setup configuration (e.g. via the circuit impedances). Extending our previous experience in trapping on semiconductor based VNDs [6, 10] we here adjusted frequency, voltage amplitude, trapping time and series resistances in such a way that a few nanoparticles were captured in the gap, however, without electrically short-circuiting the electrodes. Best results for this 'soft' trapping were obtained at 85 kHz, 4.0 V_{pp}, for 180 s with resistances 1 and 2 kΩ. An oscilloscope was connected in parallel to the latter series resistance for monitoring purposes.

Figure 3 shows an SEM image of a nanogap device with nanoparticles trapped this way onto a SAM functionalized electrode pair, thereby forming molecule–nanoparticle–molecule hybrid junctions. This particular device was

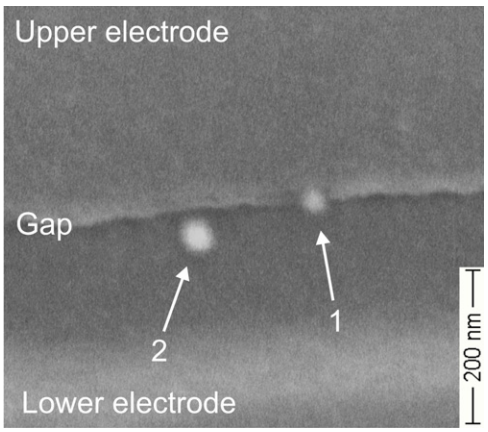

Figure 3. SEM image of part of the nanogap region of the device investigated in transport measurements, looking straight onto the plateau side wall under a viewing angle of 45°. After functionalization of the electrodes by an MCH SAM, 30 nm diameter Au nanoparticles were trapped in the gap. Clearly, two particles can be identified in this magnified view, one of them (1) positioned directly across the gap, the other one (2) located just next to it, thereby not participating in electrical conductance. Further analysis of the entire gap revealed that some ten particles were located in or on the gap in total. Note the apparent difference in nanoparticle size which can be ascribed to a different amount of charging by the SEM electron beam during observation.

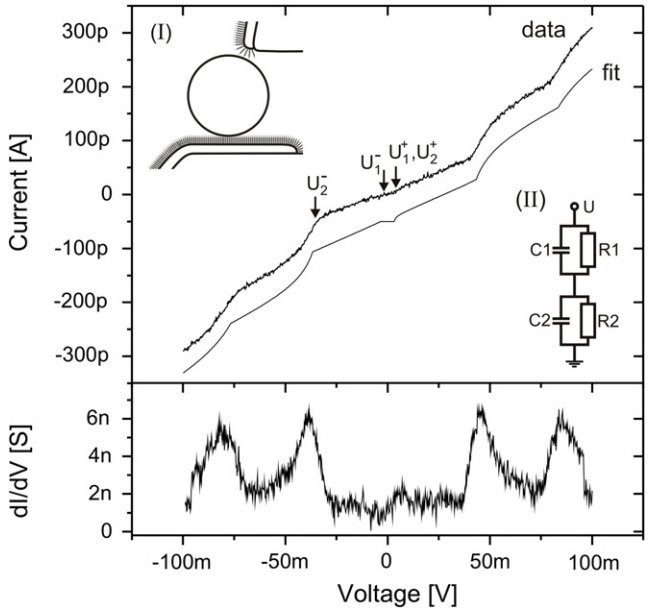

Figure 4. Upper panel: I–V characteristics ('data') of a nanogap device after electrode functionalization with an MCH SAM and subsequent trapping of 30 nm gold nanoparticles, measured at $T = 4.2$ K; simulation of the measurement ('fit', shifted by 50 pA for better visibility) within classical Coulomb blockade theory, using the following parameters (see text): $R_1 = 30$ MΩ, $R_2 = 300$ MΩ, $C_1 = 3.4$ aF, $C_2 = 4.5$ aF, $Q_0 = -0.42e$ and voltages $U_1^- = -4$ mV, $U_2^- = -33$ mV, $U_{1,2}^+ = +3$ mV as indicated close to the data trace. Insets: (I) sketch of a nanoparticle placed between functionalized electrodes of asymmetric, cross-sectional shape, cf figure 2. (II) Equivalent circuit of the double barrier tunnelling system as used in the simulation. Each SAM junction is modelled by one capacitor and one resistor in parallel. Lower panel: first derivative of the data, corresponding to the differential conductance.

investigated in the electrical transport measurements described in the following.

3.2. Electrical transport measurements

We performed electrical transport measurements on molecule–nanoparticle–molecule hybrid systems at helium temperatures (4.2 K). Figure 4 displays the current–voltage (I–V) characteristic of a vertical nanogap device after molecular functionalization (MCH SAM) and trapping of 30 nm gold nanoparticles. Compared to the device functionalized with the SAM only, the electrical properties changed dramatically upon trapping, with the resistance dropping by about two orders of magnitude down to ∼400 MΩ. Note that this resistance range contrasts with a clear short circuit on uncoated electrodes that routinely results in a linear (ohmic) I–V trace with resistances of the order of a few 100 Ω only. In particular, the measured I–V trace features a pronounced nonlinear, staircase-like characteristic. Both at positive and negative voltages step-like features can be resolved. Additional, weaker kinks are present within the region −25 to 25 mV bias. They appear more pronounced after taking the first derivative of the data, corresponding to the differential conductance (figure 4, bottom).

4. Discussion

4.1. Coulomb staircase of an asymmetric double barrier tunnelling system

The observed I–V trace is characteristic of electronic transport through a small capacitance island which is weakly coupled to the contacts via tunnelling barriers and commonly described within classical Coulomb blockade theory [15]. In the particular case of asymmetric barriers, i.e. those having strongly different resistances, the increase in bias voltage typically leads to the subsequent addition of more electrons participating in electron tunnelling. Each time the voltage is increased by another integer multiple of approximately e/C, where C is the total capacitance of the island towards its environment, the current features a step-like increase leading to an I–V trace commonly known as a Coulomb staircase. Based on the model equivalent circuit of the system (see inset II in figure 4) Hanna and Tinkham [16] showed that the particular shape of the trace may have a different appearance depending on the ratio of C_2/C_1 in relation to Q_0. Here, Q_0 is the residual fractional charge on the island, which may take values in the range $-e/2 < Q_0 < e/2$. We follow the analysis of the I–V trace given in [16] which allows for the extraction of relevant system parameters from the voltage values marking the onset of steps or kinks in the current. In general, the I–V trace exhibits a zero current plateau at small bias which relates to the Coulomb blockade of the current. The width of this plateau is determined by Q_0, while at $Q_0 = \pm e/2$ (maximum value) the plateau just vanishes, corresponding to single electron tunnelling. As evident from figure 4 our experimental situation is apparently close to this case. Hence,

the two voltages marking the first increase in current, U_1^+ and U_1^-, are located closely together and are hard to extract against the noise level. Within the uncertainty of the measurement we can estimate the upper voltage $U_2^+ = 3 \pm 1$ mV from the data. Together with the much better resolved $U_2^- = -33 \pm 1$ mV we obtain $C_2 \approx 4.5$ aF and $Q_0 \approx -0.42e$, which is very close to $-0.5e$, as expected. The remaining parameters of the equivalent circuit can be extracted with the help of a model fit to our data. Here, we used computer programs [17, 18] based on the general theory of classical Coulomb blockade, where the ratios C_2/C_1 and R_2/R_1 enter as fit parameters. As can be seen from figure 4, an apparently almost perfect agreement to the measured data could be achieved, using the parameter set $C_2/C_1 = 1.33$ and $R_2/R_1 = 10$, respectively. From the capacitance ratio and C_2 as estimated above we find $C_1 \approx 3.4$ aF. From the best fit we furthermore extract the value $U_1^+ \approx 3$ mV (identical to U_2^+), and $U_1^- \approx -4$ mV which could not be directly read from the data. Once the capacitances have been extracted, the resistances follow from the slopes on a step with constant fractional charge according to $\partial I/\partial V = C_1/(R_2 C_\Sigma)$ with $C_\Sigma = C_1 + C_2$. A linear fit to the data in the interval 5–30 mV yields $R_2 \approx 300$ MΩ. Using $R_2/R_1 = 10$ from the fit we obtain $R_1 \approx 30$ MΩ, hence $R_\Sigma = R_1 + R_2 = 330$ MΩ which is in reasonable agreement with the average sample resistance $I/V \approx 380$ MΩ taken over the whole measurement range $V = \pm 100$ mV.

4.2. Basic model for estimating the fit parameters

Using a simple physical model of the hybrid system consisting of electrodes, SAM and nanoparticles most of the parameters making up the equivalent circuit can be independently estimated and compared to the parameters derived from the model fit. In a first approximation the conductance for electrons tunnelling through a single alkyl chain molecule like MCH may be estimated using the Landauer formula $G = G_0 \exp(-\beta d)$, where $G_0 = 2e^2/h$ is the conductance quantum. Here, the film thickness $d = 1.0$ nm enters as the tunnelling distance and β is the tunnelling decay parameter. For alkyl molecules, a large number of transport measurements have been reported in the literature, which have extracted β values mostly in the range from about 0.5 to 1 Å^{-1} [19, 20]. The value of $R_2 = 300$ MΩ as obtained from our model fit corresponds roughly to $\beta \approx 1$ Å^{-1}. Since this value of β is located at the upper bound of the reported range, we may conclude that one of our electrodes contacts the nanoparticle via at most a few but probably just one, single molecule. Due to the exponential dependence of the tunnelling resistance as a function of β, a more accurate estimate is beyond the scope of our analysis. However, we note that a relatively high β value may well be expected in our experiment since only one side of each MCH molecule is specifically bound to gold while the –OH group at the other (nanoparticle) side presumably creates an additional barrier to electron tunnelling [21]. The occurrence of the Coulomb staircase must originate from strongly asymmetric tunnelling resistances of both junctions to the nanoparticle, which is reflected in the one order of magnitude lower resistance R_1 obtained from the model fit, as compared to R_2. This asymmetry is directly evident from the different shapes of the two electrodes, as visible in the cross-sectional image of figure 2. While the upper electrode has a sharply limited linear shape, its opposing lower electrode features a smoothly rounded, comparably planar geometry. As sketched in figure 4, inset I, we anticipate that mainly this dissimilar geometry is responsible for the observed, pronounced asymmetry in resistances, and conclude that of the order of ten molecules in parallel may contribute to the lower junction resistance[4]. The capacitance of an isolated sphere of diameter $r = 15$ nm in vacuum is $C = 4\pi\epsilon_0 r \approx 1.7$ aF, a value which already fits the order of magnitude of the derived capacitances very well. While for the upper contact only minor enhancing corrections may be expected due to the line shape of this electrode, the corrections for the lower contact may be anticipated to be larger. Considering a sphere opposing a flat surface in a distance of $d = 1.0$ nm we estimate $C = 2\pi\epsilon_0 r \ln(1 + \frac{r}{d}) \approx 2.3$ aF [22], which exceeds the estimated capacitance of the upper junction by a factor of ∼1.35, in very good agreement with the ratio derived from fitting the data: $C_2/C_1 = 1.33$.

We finally note that some ten nanoparticles in total were identified in the gap region of the investigated sample. The actual number of particles contributing to transport, however, cannot be concluded from SEM imaging only. Our analysis employing the theoretical model together with the independent estimation of the physical parameters confirms our assumption of a single contributing hybrid system only.

5. Conclusions

We fabricated vertical nanogap electrode devices (VNDs) from SOI substrates using standard silicon microelectronic process technology. STEM analysis revealed the high structural quality of the fabricated electrode pairs with separation down to 26 nm. By coating the electrodes with a mercaptohexanol SAM and trapping 30 nm diameter gold nanoparticles dielectrophoretically we formed molecule–nanoparticle hybrid systems and investigated their electronic transport properties at $T = 4.2$ K. The measured Coulomb staircase I–V characteristic indicated an asymmetric double barrier tunnelling system. We find our data in excellent agreement with available model calculations within classical Coulomb blockade theory, supporting this interpretation. A fit to the data yielded capacitances of comparable magnitude $C_1 \approx 3.4$ aF and $C_2 \approx 4.5$ aF, for both junctions, however strongly differing junction resistances $R_1 \approx 30$ MΩ and $R_2 \approx 300$ MΩ, respectively were deduced from the same fit. An independent estimate of the order of magnitude of these parameters based on simple model considerations strongly supports these findings. The observed asymmetry in junction resistances can be clearly assigned to the dissimilar shape of both electrodes. In summary, we presented a reproducible and

[4] We note that ten molecules contacted in parallel at the lower junction would cover a circular area of about 1.5 nm diameter on the 30 nm nanoparticle surface, taking into account the average footprint area of molecules in alkyl SAMs [11]. This finite area junction would imply the nanoparticle imprinting the SAM by about 2% of its thickness, a value which appears reasonably small considering the compactness of alkyl SAMs.

systematic way of fabricating nanogap electrode devices fully compatible with silicon process technology and demonstrated their applicability for the controlled investigation of transport phenomena in nanoscale objects.

Acknowledgments

This work was financed by the BMBF under grants 03N8713 and 03X5513 (Junior Research Group 'Nanotechnology'), by the Fujitsu Laboratories of Europe and the Nanosystems Initiative Munich (NIM). We acknowledge G Abstreiter for his support of our work and many fruitful discussions. We thank A Korotkov and R Krahne for helpful support regarding the data fitting, D Grundler and P Berberich for access to the SEM and Zeiss SMT AG Oberkochen for STEM analysis. RHM acknowledges support by the Erasmus student exchange program and by the Telecommunication School at UPCT (Spain).

References

[1] ITRS: The International Technology Roadmap for Semiconductors http://www.itrs.net/
[2] Reed M A and Lee T 2003 *Molecular Nanolectronics* (Los Angeles, CA: American Scientific Publishers)
[3] Ellenbogen J C and Love J C 2000 Architectures for molecular electronic computers: 1. Logic structures and an adder designed from molecular electronic diodes *Proc. IEEE* **88** 386–426
[4] Tao N J 2006 Electron transport in molecular junctions *Nat. Nanotechnol.* **1** 173–81
[5] Krahne R, Yacoby A, Shtrikman H, Bar-Joseph I, Dadosh T and Sperling J 2002 Fabrication of nanoscale gaps in integrated circuits *Appl. Phys. Lett.* **81** 730–2
[6] Luber S M, Strobel S, Tranitz H P, Wegscheider W, Schuh D and Tornow M 2005 Nanometre spaced electrodes on a cleaved AlGaAs surface *Nanotechnology* **16** 1182–5
[7] Luber S M, Zhang F, Lingitz S, Hansen A G, Scheliga F, Thorn-Csanyi E, Bichler M and Tornow M 2007 High-aspect-ratio nanogap electrodes for averaging molecular conductance measurements *Small* **3** 285–9
[8] Sazio P J A, Berg J, See P, Ford C J B, Lundgren P, Greenham N C, Ginger D S, Bengtsson S and Chin S N 2001 A silicon structure for electrical characterisation of nanoscale elements *MRS Spring Mtg* (San Francisco, CA: Materials Research Society) p B2.3.1
[9] Dirk S M, Howell S W, Zmuda S, Childs K, Blain M, Simonson R J and Wheeler D R 2005 Novel one-dimensional nanogap created with standard optical lithography and evaporation procedures *Nanotechnology* **16** 1983–5
[10] Strobel S, Arinaga K, Hansen A and Tornow M 2007 A silicon-on-insulator vertical nanogap device for electrical transport measurements in aqueous electrolyte solution *Nanotechnology* **18** 295201
[11] Schreiber F 2000 Structure and growth of self-assembling monolayers *Prog. Surf. Sci.* **65** 151–256
[12] Miller C, Cuendet P and Gratzel M 1991 Adsorbed omega-hydroxy thiol monolayers on gold electrodes—evidence for electron-tunneling to redox species in solution *J. Phys. Chem.* **95** 877–86
[13] Amlani I, Rawlett A M, Nagahara L A and Tsui R K 2002 An approach to transport measurements of electronic molecules *Appl. Phys. Lett.* **80** 2761–3
[14] Barsotti R J, Vahey M D, Wartena R, Chiang Y M, Voldman J and Stellacci F 2007 Assembly of metal nanoparticles into nanogaps *Small* **3** 488–99
[15] Averin D V and Likharev K K 1991 *Mesoscopic Phenomena in Solids* ed B L Altshuler *et al* (Amsterdam: Elsevier) p 173
[16] Hanna A E and Tinkham M 1991 Variation of the Coulomb staircase in a 2-junction system by fractional electron charge *Phys. Rev.* B **44** 5919–22
[17] Hadley P Single-electron device java simulation programs http://med.tn.tudelft.nl/~hadley/index1.html
[18] Korotkov A N 1994 Intrinsic noise of the single-electron transistor *Phys. Rev.* B **49** 10381–92
[19] Salomon A, Cahen D, Lindsay S, Tomfohr J, Engelkes V B and Frisbie C D 2003 Comparison of electronic transport measurements on organic molecules *Adv. Mater.* **15** 1881–90
[20] Akkerman H B and de Boer B 2008 Electrical conduction through single molecules and self-assembled monolayers *J. Phys.: Condens. Matter* **20** 013001
[21] Wang G, Kim T W, Lee H and Lee T 2007 Influence of metal–molecule contacts on decay coefficients and specific contact resistances in molecular junctions *Phys. Rev.* B **76** 205320
[22] Hudlet S, Saint Jean M, Guthmann C and Berger J 1998 Evaluation of the capacitive force between an atomic force microscopy tip and a metallic surface *Eur. Phys. J.* B **2** 5–10